Coarse-grained molecular dynamics of ligands binding into protein: The case of HIV-1 protease inhibitors

Dechang Li,[1] Ming S. Liu,[2,3,a)] Baohua Ji,[1,b),a)] Kehchih Hwang,[1] and Yonggang Huang[4,a)]

[1]*Department of Engineering Mechanics, School of Aerospace, Tsinghua University, Beijing 100084, China*
[2]*Centre for Molecular Simulation, Swinburne University of Technology, P.O. Box 218, Hawthorn 3122, Australia*
[3]*CSIRO Mathematical and Information Sciences, Private Bag 33, Clayton South 3169, Australia*
[4]*Department of Civil and Environmental Engineering, Northwestern University, Evanston, Illinois 60208, USA*

Binding dynamics and pathways of ligands or inhibitors to target proteins are challenging both experimental and theoretical biologists. A dynamics understanding of inhibitors interacting with protein is essential for the design of novel potent drugs. In this work we applied a coarse-grained molecular dynamics method for simulating inhibitors entering the binding cavity of human immunodeficiency virus type 1 protease (PR). It shows that the coarse-grained dynamics, consistent with the experimental results, can capture the essential molecular dynamics of various inhibitors binding into PR. The primary driving force for the binding processes is the nonbond interaction between inhibitors and PR. The size and topology of inhibitors and the interacting strength between inhibitors and PR have great influence on the binding mode and processes. The interaction strength between the PR and various inhibitors is also analyzed by atomistic molecular mechanics and Poisson–Boltzmann solvation area method. © *2009 American Institute of Physics.*
[DOI: 10.1063/1.3148022]

I. INTRODUCTION

Conformational dynamics plays essential roles in regulating protein functions.[1,2] How protein dynamics, arising from ligands binding into proteins, protein docking with DNA/RNA, and protein-protein interactions, would affect the functions have been far beyond understanding both experimentally and theoretically. For a wide range of protein functions, dynamics and pathways of ligands or inhibitors binding to proteins are especially challenging since ligand binding and inhibition induce collective dynamics and large-scale conformational changes in the target proteins. For example, proteins will undergo (a) conformational transition between distinctive states; (b) allostery and cooperativity of multisite activities or intersubunit interactions in a multimeric protein. At the same time, flexibility, fluctuations, and correlated dynamics of proteins are intrinsically regulated by ligands binding or inhibition activities. A understanding of dynamics collectivity, transition pathways and correlations is vital for understanding protein functions,[3] signaling networks, enzyme activity, and more practically for the design of novel potent drugs.[4]

For the study of ligand-protein binding and interaction dynamics, we chose human immunodeficiency virus type 1 protease (HIV-1 PR) as a model system. HIV-1 PR has a critical role in the virus replication cycle that cleaves the *gag* and *pol* viral polyproteins at the active site to process viral maturation.[5–7] It was found that the virus without HIV-1 PR is noninfectious.[8] Thus HIV-1 PR is continuously considered the primary target for the AIDS treatment.[9,10] However, the effectiveness of the inhibitors is reduced gradually (since the PR mutates frequently during inhibitor therapy),[11,12] and novel potent inhibitors are constantly explored for an improved and hopefully ultimate AIDS treatment. For this purpose, a molecular understanding of binding and inhibiting dynamics of potential inhibitors to PR is both fundamental and practical to the HIV-1 PR drug design.

HIV-1 PR is a dimeric aspartic PR [Fig. 1(a)] with each monomer containing about 99 residues and the active site caved by two flexible β-hairpin flaps (i.e., residues 43–58). The crystallographic and NMR structures showed that HIV-1 PR exists in large ensemble of conformations, mainly distinctive for a semiopen state [i.e., Fig. 1(a), with the flaps packed loosely[13]] and a closed state [i.e., Fig. 1(a), with the inhibitors or substrates bound at the active site and the flaps packed tightly[14,15]]. It was expected that there should be an open configuration where flaps open wide (e.g., distance between the flap tips >20 Å), but it is not observed in experiments.[16,17] NMR studies indicated that the flaps move at microsecond time scale, while the flap tips undergo conformational exchanges on nanosecond timescale in free HIV-1 PR.[18–21] The dynamics of flaps are much constrained when inhibitors or substrates bind into the cavity site. Apparently flexibility and dynamics of flaps and ligands play key roles in the HIV-1 PR inhibition processes. Lots of effort in

---

a)Authors to whom correspondence should be addressed. Electronic addresses: mliu@swin.edu.au or ming.liu@csiro.au, bhji@bit.edu.cn, and y-huang@northwestern.edu.
b)Present address: Department of Applied Mechanics, Beijing Institute of Technology, Beijing 100081, China.
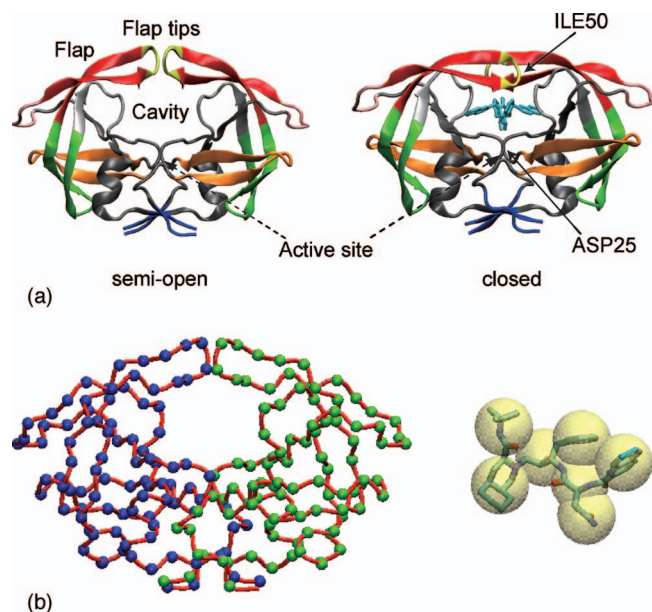
FIG. 1. (Color) (a) HIV-1 PR has distinct conformational states as determined by structural experiments, namely, a semiopen free PR (e.g., PDB:1HHP, with a distance between the flap tips of about 4.3–14 Å) and an inhibitor-bound closed PR (e.g., PDB:1HVR, with distance between the flap tips is <5.8 Å). The colors indicate different structure regions as defined (Ref. 31) the flaps (red), flap tips (yellow), flap elbow (pink), cantilever (green), and dimer interface (cyan), respectively; (b) CG treatment of HIV-1 PR, where atomic details are CG by hard sphere beads of amino acids. Ligand SQV (right) as a potential inhibitor, where the functional group in the dashed ellipse is CG as hard sphere beads (more details see supplementary Fig. 1) (Ref. 87).

both experiments[19,20,22–25] and molecular dynamics (MD) simulations[26–32] were paid to HIV-1 PR to reveal its open/close dynamics, intrinsic correlated motions, and free energy changes. However, a full molecular understanding of the ligand binding and inhibition remains unsolved. Particularly for MD simulations of HIV-1 PR, the complete binding processes are challenging all-atom simulations because of the time scale and size limitation.[23,33,34] Experiments suggested that the ligands bind to PR may follow either a two-step or one-step mechanism.[24,25] This experimental finding denounced the validity of previous all-atom simulations on inhibiting mechanism and dynamic pathways. Thus new simulation algorithms, such as multiscaled coarse-grained (CG) methods,[35] should be developed for a molecular simulation of ligands binding and inhibition dynamics of HIV-1 PR.

Similarly, the theoretical barriers and difficulties in simulating HIV-1 PR also occur generally in other ligand-protein complexes. In this work, using HIV-1 PR as a model system, we applied a CG dynamics algorithm to overcome the problems arising from all-atom MD simulation. There are different level CG models developed for proteins. For example, the first CG model might be the "one-bead" models, where each amino acid residue is CG as one bead placed at the C-alpha position.[36–38] To consider more details of side-chain effect, "two-bead" model was developed with additional bead to the one-bead model.[39,40] Moreover the two-bead models were further extended to three-bead, four-bead, and six-bead models in more detailed backbone and side-chain interactions (such as the mimicked hydrogen

bonds).[41–46] To consider as much as accurate conformational terms than simple bead-networked models, an improved CG method was tested for effectively simulating ligand binding dynamics and product release in HIV-1 PR up to microsecond time scale.[32,47–51] We now adopt a similar CG strategy and optimize further a set of CG force field parameters for both proteins and ligands, as well as their interactions. The methods allowed us not only to analyze the binding pathways of inhibitors to HIV-1 PR but also other factors such as driving forces strength, the inhibitor size, and topology. This will help for a much insightful understanding of ligand binding into target proteins and further inhibition.

II. ALGORITHMS AND METHODS

A. Coarse-grained models of HIV-1 PR and inhibitors

Atomistic details of HIV-1 PR and the inhibitors were CG as hard sphere beads. For the PR, as shown in Fig. 1(b), each amino acid is represented as one sphere bead of different size and weight. The effective radii of beads were taken from the widely accepted definition by Reva *et al.*,[52] and the bead is placed at the C-alpha position and connected by virtual bonds, angles, and dihedral angles. The inhibitors were also CG as hard sphere beads [for details, see Eqs. (4) and (5) and in supplementary Fig. 1 (Ref. 87)] representing different functional groups of the inhibitor.

With the CG treatment, total potential function (i.e., the CG force field) for HIV-1 PR is a sum of the following interactions:[47,48]

$$U = U_{\text{bond}} + U_{\text{angle}} + U_{\text{dihedral}} + U_{\text{el}}^{\text{nonlocal}} + U_{\text{nb}}^{\text{local}} + U_{\text{nb}}^{\text{nonlocal}},$$

(1)

where U_{bond}, U_{angle}, and U_{dihedral} potentials are the bonded interactions and the rest terms are the nonbonded interactions.

The bonded and dihedral interactions, U_{bond} and U_{dihedral}, follow a harmonic format[48] while U_{angle} takes a quadratic double-well type (which is mainly responsible for the conformational changes involved in α-helix to β-sheet). In this work, we adopted the same process designed by Tozzini *et al.*[48] in parametrizing U_{bond}, U_{angle}, and U_{dihedral}. For nonbonded interactions, $U_{\text{el}}^{\text{nonlocal}}$ is the electrostatic interaction function where a distance-dependent dielectric coefficient (i.e., $\varepsilon_{ij} = 4r_{ij}$) mimics the aqueous environment. For the charges of the CG beads of 20 amino acids, they take integer values of -1, -1, $+1$, and $+1$ for Asp, Glu, Lys, and Arg (according to their protonation in solution at pH7), respectively, while other amino acids are treated as neutral. Meanwhile a Morse potential was applied to the local and nonlocal nonbonded interaction functions of $U_{\text{nb}}^{\text{local}}$ and $U_{\text{nb}}^{\text{nonlocal}}$, respectively. The local nonbonded interactions can break during simulation and nonlocal interactions can form, thus allow large conformational changes,

$$U_{nb} = \begin{cases} U_{nb}^{local} = \beta[(1 - e^{-\alpha(r_{ij}-r_0)})^2 - 1] & \text{for } r_{ij} \leq 8 \text{ Å}, \\ U_{nb}^{nonlocal} = 0.207\,08[(1 - e^{-\alpha(r_{ij}-9.75)})^2 - 1] & \text{for } 8 \text{ Å} \leq r_{ij} \leq 15 \text{ Å}, \end{cases} \quad (2)$$

where r_{ij} is the distance between two beads and r_0 is equilibrium position within the critical distance 8 Å from local to nonlocal, which was taken from the average semiopen state of PR (e.g., PDB code: 1HHP). The fitting parameter α was set as 0.707 11/Å, and $\beta = 6\exp(-r_0/2.8)$ kcal/mol.[48] Other parameterization details of the CG treatment can also refer to the works of Tozzini et al.[47,48]

B. The interaction between HIV-1 PR and inhibitors

To coarse-grain the inhibitors into a branched sphere beads, the topology of inhibitors was taken from the corresponding Protein Data Bank (PDB) coordinates. The bonded terms of its force field including bond, angle, and dihedral angle potentials were treated as harmonic. The CG beads and strength parameters of the potentials were set, as shown in supplementary Tables I and II,[87] respectively.

The interactions between HIV-1 PR and the inhibitor are treated as a modified Lennard-Jones (LJ) potential,[51,53]

$$U_{vdw}^{inter} = \varepsilon\left[\left(\frac{R_i + R_j}{r_{ij}}\right)^8 - 1.5\left(\frac{R_i + R_j}{r_{ij}}\right)^6\right], \quad (3)$$

where r_{ij} is the distance from bead i to j, while R_i and R_j are the effective radii of bead i in PR and bead j in inhibitor, respectively. The strength of the interactions is defined by the parameter ε. Different from previous studies,[51] we used the interaction energy of varied inhibitors calculated in all-atom models to determine the value of ε, and the effect of the interaction strength will be discussed in more details in Sec. III. For the inhibitors, the effective radius of bead is defined as

$$R_j^{eff} = R_j^g + R_{CH}^{Vdw}, \quad (4)$$

in which R_j^g is radius of gyration of CG bead j, which can be calculated by

$$R_j^g = \left(\sum_m^N r_{mj}\right)\bigg/ N, \quad (5)$$

where r_{mj} represents the distance between heavy atom m within the CG bead j and the geometry center of the CG bead, and N is the total number of heavy atoms within the bead, respectively. R_{CH}^{Vdw} is the average Van der Waals (Vdw) radii of $CH/CH_2/CH_3$ groups which are located at the most outside of the CG beads. R_{CH}^{Vdw} is equal to 1.925 Å.[54] The parameters of the effective radii of beads in inhibitors' CG models are showed in supplementary Table I.[87]

C. Calculation of interaction energy

In order to investigate the driving forces, association rate and affinity for the binding processes, we calculated the interaction energy of inhibitors binding by all-atom molecular mechanics (MM) and Poisson–Boltzmann solvation area method.[55] The binding free energy consists of the following parts:

$$\Delta G_b = \Delta U - T\Delta S = \Delta G_{MM} + \Delta G_{sol}^C - \Delta G_{sol}^P - \Delta G_{sol}^I - T\Delta S, \quad (6)$$

where ΔU is interaction energy, given by $\Delta U = \Delta G_{MM} + \Delta G_{sol}^C - \Delta G_{sol}^P - \Delta G_{sol}^I$, and ΔG_{MM} is the interaction energy between the PR and the inhibitor; ΔG_{sol}^C, ΔG_{sol}^P, and ΔG_{sol}^I are the solvation free energy for the PR-inhibitor complex, PR itself, and the inhibitor itself, respectively. The term of $-T\Delta S$ reflects the conformational entropy changes upon binding.

ΔG_{MM} can be further decomposed into Vdw and electrostatic parts,

$$\Delta G_{MM} = \Delta G_{int}^{vdw} + \Delta G_{int}^{ele}. \quad (7)$$

The solvation energy ΔG_{sol} consists of two parts, the electrostatic contribution and the nonpolar contribution, as

TABLE I. Interaction energies for potential HIV-1 PR inhibitors. (Data in parentheses are from Refs. 32, 51, and 60.)

Inhibitors	ΔG_{MM} Vdw (kcal/mol)	Electrostatic (kcal/mol)	ΔG_{sol} Nonpolar (kcal/mol)	Polar (kcal/mol)	ΔU (kcal/mol)	ε_0 value in CG models (kcal/mol)	LJ potential energy in CG models (kcal/mol)
XK263	-69.7 ± 3.8	-38.7 ± 2.0	-6.0 ± 0.2	76.2 ± 1.9	-38.2 ± 2.8 $(-30 \sim -40)$	0.46	-37.63 ± 0.2
NFV	-64.1 ± 3.0 (-65.3 ± 2.3)	-38.5 ± 2.5 (-36.8 ± 0.8)	-6.0 ± 0.3 (-5.7 ± 0.0)	84.3 ± 2.5 (82.8 ± 0.8)	-24.3 ± 2.2 (-26.8 ± 0.1)	0.32	-25.66 ± 0.2
SQV	-59.1 ± 2.5 (-67.6 ± 0.3)	-30.9 ± 2.5 (-24.6 ± 1.9)	-6.7 ± 0.3 (-6.6 ± 0.1)	69.2 ± 2.4 (72.0 ± 2.0)	-27.5 ± 2.7 (-25.1 ± 0.6)	0.29	-27.53 ± 0.3
QF34	-67.6 ± 2.5	-50.1 ± 2.3	-7.1 ± 0.2	97.2 ± 3.0	-27.6 ± 3.0	0.24	-27.12 ± 0.3

TABLE II. Association rate constants and binding times of different inhibitors.

	Association rate constants $(M^{-1}\,s^{-1})$	Estimated binding time[a] (ns)
XK263[b]	$2.52 \times 10^{10} \pm 9.99 \times 10^{9}$	~15
NFV	$6.63 \times 10^{5} \pm 3.04 \times 10^{5}$	~130
SQV	$8.17 \times 10^{5} \pm 1.61 \times 10^{5}$	~250
QF34	n.a.	~250

[a]Binding time is an approximate indication of the binding capability when the inhibitors are set at the same initial position under same boundary conditions.
[b]The association rate constants were from Ref. 22. As no experimental results for XK263 were determined, the rate constant of XK263 was fitted from its analoglike ligand of DMP323.

$$\Delta G_{sol} = \Delta G_{sol}^{ele} + \Delta G_{sol}^{nonpolar}. \tag{8}$$

Here the energy ΔG_{sol}^{ele}, reflecting the polar solvation energy, was calculated by solving the Poisson–Boltzmann equations using the APBS package.[56] With the grid size set to 0.5 Å, the interior dielectric constant was set to 1 while the dielectric constant of water was set to 80. The radii of atoms were taken from the AMBER parameters by the PDB2PQR method.[57] The nonpolar contribution, corresponding to the burial of the solvent-accessible surface area (SASA) upon binding, was calculated by

$$\Delta G_{sol}^{nonpolar} = \gamma \times SASA + \eta, \tag{9}$$

where SASA was the solvent-accessible surface area that was calculated by the MSMS program[58] with 1.4 Å radius probe sphere. γ (set to 0.00542 kcal/mol Å^2) and η (set to 0.92 kcal/mol) are the constants extracted from a least-squares fit to a plot of experimental alkane transfer free energies versus accessible surface area.[59,60]

D. CG and atomistic MD simulations details

The CG simulations were performed on the GROMACS-3.3.1 platform[61,62] in which a Langevin dynamics (LD) module was applied for mimicking frictional and stochastic effects of the solvent. The Langevin equation of motion is

$$m_i \frac{d^2 r_i}{dt^2} = F_i(r) - \gamma m_i \frac{dr}{dt} + R_i(t), \tag{10}$$

where m_i is the mass of the CG bead, $F_i(t)$ is the systematic force, γ is the collision frequency, and $R_i(t)$ is a noise process with $\langle R_i(0)R_j(t)\rangle = 2m_i\gamma k_B T \delta_{ij}(t)$, where k_B is the Boltzmann constant and T is the absolute temperature. The γ parameter determines both the magnitude of the friction and the variance of the random force. In LD simulations, we set the collision frequency parameter γ to 2/ps as previously reported,[32] and the time step was set to 10 fs (due to the flexible force field in CG model and the large mass of CG beads, this large time step is justified). The simulation temperature was set to 300 K. The nonbonded pair list was updated every five steps. The nonbonded interaction cutoff between the CG beads of the PR and the inhibitors was set to 20 Å. The parameterization of CG force field was first fitted by Tozzini and co-workers[48,51] in using DL_POLY (Ref. 63)

and UHBD package.[64] We here implemented the CG force field into the GROMACS-3.3.1. More parameters details see supplementary Tables I and II.[87]

The starting free state of PR for CG simulations was chosen as the semiopen structure (PDB code: 1HHP). The inhibitor-bound structures were retrieved from Protein Data Bank with PDB codes of PDB:1HVR (Ref. 14) for XK263, PDB:1OHR (Ref. 65) for NFV, PDB:1HXB (Ref. 66) for SQV, and PDB:1IZH (Ref. 67) for QF34. Several side chains of the PR were modified to match the sequence of PDB:1HHP.

All-atom simulations were also performed using GROMACS-3.3.1 (Refs. 61 and 62) with the force field of ffamber99.[68] The all-atom force field parameters of inhibitors were obtained by the ANTECHAMBER module and general AMBER force field (Refs. 69 and 70) with AM1-BCC (Ref. 71) charges in AMBER package.[72] Both catalytic Asp side chains of the PR were modeled in the nonprotonated state according to the protonation in solution at pH 7. The HIV-1 PR systems were solvated in an $90 \times 80 \times 80$ Å^3 TIP3P water box.[73] Appropriate Cl ions were added to neutralize the system. Particle mesh ewald[74] was used to calculate the long-range electrostatic interactions. The systems were minimized and then gradually heated to 300 K and equilibrated in 200 ps. Positional restraints were used first and the restraint force constants were decreased from 2.39 to 0 kcal/mol Å^2 in a few stages. All production simulations were at 300 K with a pressure of 1 bar with the Berendsen algorithm[75] and last 1 ns. The SHAKE algorithm[76] was applied to constrain the bonds with H-atoms. The time step of the simulations is 2.0 fs. The cutoff of the nonbonded interactions was set to 10 Å. The nonbonded pairs were updated every ten steps. The 1 ns simulation trajectories were saved as 500 snapshots, and the last 250 snapshots were used to calculate the interaction energy ΔG_{MM} and ΔG_{sol}. All graphics and visualization analysis were processed using the VMD program.[77]

III. RESULTS AND DISCUSSIONS

A. CG dynamics of free HIV-1 PR

To validate the CG force field we implemented, we herein first investigate the opening and closing dynamics of the ligand-free HIV-1 PR, e.g., the dynamics of two flaps without ligands. As shown in Fig. 2, CG simulations produce the same-level accuracy on conformational dynamics of HIV-1 PR, in terms of fluctuations, collectivity, and flexibility, as of the all-atom simulations.

A typical trajectory of the CG dynamics of HIV-1 PR is showed in Fig. 3(a). The large lateral movements of flaps are the primary motions, and CG dynamics show that the PR flaps can dynamics-driven transit between the open, semiopen, and close states constantly. Because the active site is caved by two flaps, the accessibility of the substrates or inhibitors was normally marked out by a key distance of between tips of ILE50A-ILE50B.[29,31,48] Here, we found that the distance between the active site and the flap tips, which denoted by the ASP25A-ILE50A distance, is also a very important measure of the flapping dynamics. In fact, the binding accessibility of inhibitors should be a combination of the
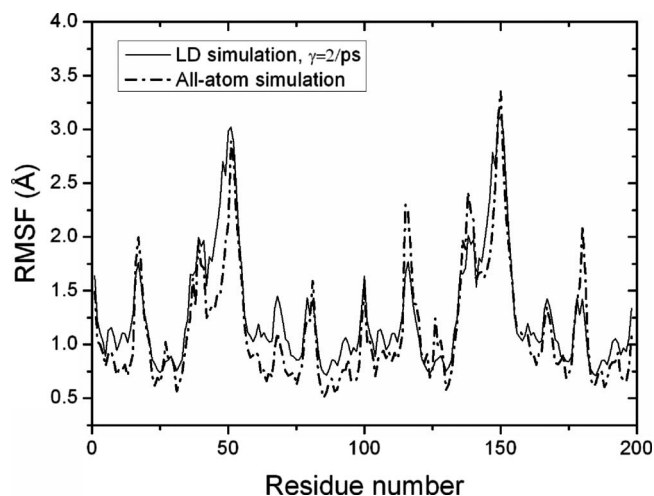
FIG. 2. CG simulations produce the same-level conformational dynamics of HIV-1 PR, in terms of fluctuations, collectivity, and flexibility, as of the all-atom simulations.

ILE50A-ILE50B and ASP25A-ILE50A distances that gives an actual volume and space of the binding cavity. Thus we define the open state of PR as a state when a correlated opening of the ILE50A-ILE50B (i.e., >14 Å) and ASP25-ILE50 (i.e., >18 Å) distances occurs simultaneously.
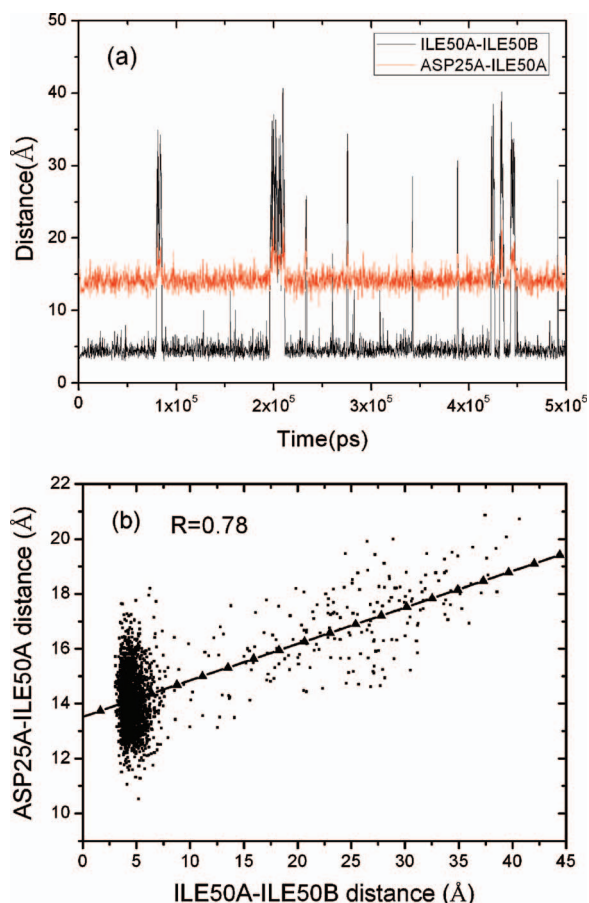

FIG. 3. (Color) CG dynamics of free HIV-1 PR in a 500 ns timeframe: (a) trajectories of distances of ILE50A-ILE50B and ASP25A-ILE50A (the LD simulation with collision frequency 2/ps, output every 200 ps, time step is 10 fs). (b) Correlation of the ILE50A-ILE50B and ASP25A-ILE50A distances. The line was fitted linearly with a correlation coefficient $R=0.78$.

Our definition of the open state is justified by the positive correlation between the ASP25A-ILE50A distance and the ILE50A-ILE50B distance [Fig. 3(b)]. The two distances are correlated linearly with a correlation coefficient of $R=0.78$. This indicates that the depth of the active site cavity shall move coupled to the width of the flaps tips, thus the potential substrates or inhibitors can access a fully opening active site pocket.

B. CG dynamics of inhibitors binding into HIV-1 PR

We investigated the CG dynamics of two kinds of promising inhibitors for HIV-1 PR: The small ligands with no flap water (e.g., XK263, DMP323, and DMP128), and the large ligands with flap water (e.g., SQV, NFV, and QF34).[78]

Figures 4 and 6 show the inhibiting dynamics trajectories (translated by key flapping distances of ILE50A-ILE50B, ASP25A-ILE50A, and ASP25A-inhibitor; as well as interaction energies) of test inhibitor XK263 and Food and Drug Administration (FDA)-approved saquinavir (SQV) binding into ligand-free HIV-1 PR, respectively. Meanwhile, Figs. 5 and 7 record a series of conformational snapshots in their corresponding binding pathways, respectively.

To reveal the binding processes of inhibitors, the inhibitors was randomly put outside the binding cavity (about 20 Å away), as presented in Figs. 5 and 7 at $t=0$. Given that the active site of HIV-1 PR is formed by six amino acids that construct two triads of Asp-Thr-Gly (residue numbers 25–27 and $25'-27'$) at each monomer,[6] we use the distance of ASP25A-inhibitor to describe the position of inhibitor related to the active site. The ASP25A-inhibitor distance is defined as the distance between ASP25 of monomer A and the mass center of inhibitor, and it is the structural indicator of the binding dynamics.

For the binding dynamics and inhabitation pathways of XK263, XK263 first rotated a lot for a correct orientation and close contact with the cavity. The inhibitor posed to enter the cavity by collisions with the PR until the opening of the flaps (e.g., in Fig. 5, $t=15.66$ ns for XK263 when both the distances of ILE50A-ILE50B and ASP25A-ILE50A open). During the time from 15 to 45 ns with the flaps open, XK263 rearranged its orientation in the cavity until forming a tightly packed complex with PR and the flaps fully closed (at $\sim t=45$ ns with the mean distance of ASP25A-XK263 around 10 Å, and ILE50A-ILE50B returned to about 5 Å). The flaps do not open again till the simulation ended at $t=500$ ns (Fig. 4, with results up to 75 ns showed). To confirm the correlation between ILE50A-ILE50B and ASP25A-ILE50A distances during the binding process, we draw the distribution of ILE50A-ILE50B versus ASP25A-ILE50A distances in the binding process of XK263, as showed in Fig. 4(c). There is clear correlation (with a correlation coefficient $R=0.77$) between the ILE50A-ILE50B and ASP25A-ILE50A distance during XK263 binding into the active site.

It should be noted that the current CG treatment does not catch the specific interactions between the flap tips and those between flap tips and inhibitors at atomistic level. Although the flap reversal can sometimes happen (as shown in Fig. 2 with different flap handednesses[87]), it does not help define
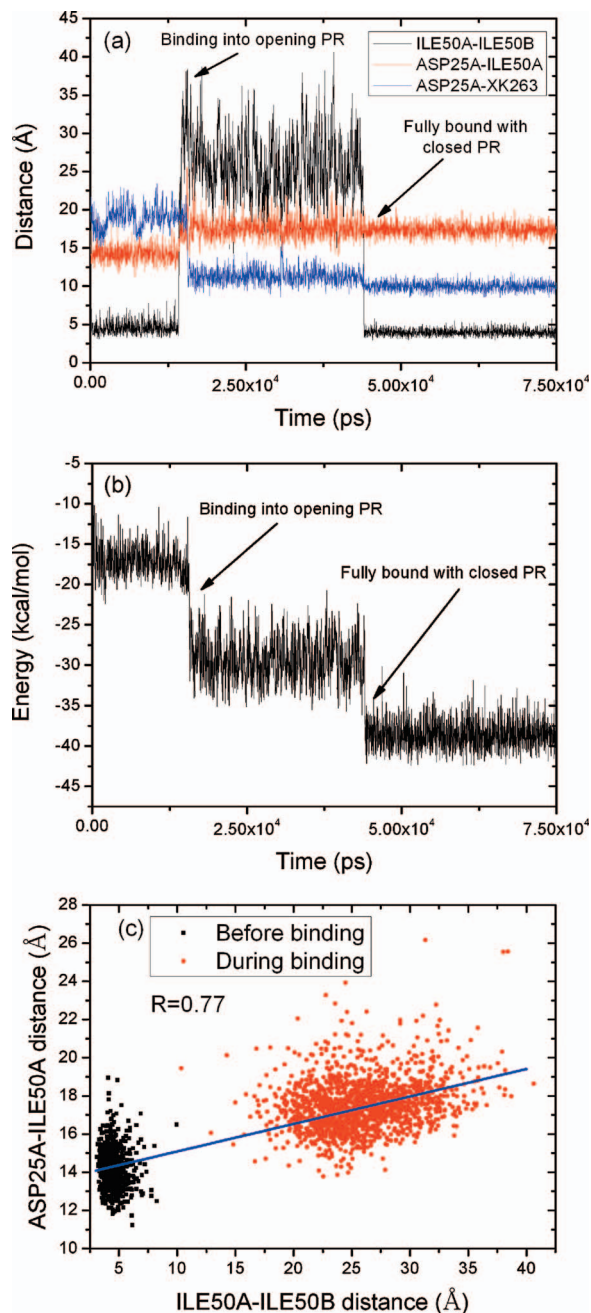
FIG. 4. (Color) Binding dynamics of substrate XK263. (a) Distances of ILE50A-ILE50B, ASP25A-ILE50A, and ASP25A-XK263 obtained in the LD simulation with collision frequency 2/ps, output every 20 ps, time step is 10 fs—the stepping of distances mark out different stages of binding. (b) Accompanying the binding process of inhibitors, there is a significant changes in the total interaction energy between XK263 and the PR dropped from ~−10 to −17 kcal/mol as the binding begins, decreased to ~−30 kcal/mol as the flaps open, and stabilized to −38 kcal/mol for fully bound. (c) Correlation of the ILE50A-ILE50B and ASP25A-ILE50A distances in the binding process of XK263 with the flaps opened. The black data points represented the process before binding, while the red data points represented the process during binding. The blue line was fitted with a correlation coefficient $R=0.77$.

the semiopen and closed configuration in the dynamics simulation. Instead, we used the distances of ILE50A-ILE50B and ASP25A-ILE50A to describe the accessibility of the active site. In this study, we focused on the entering dynamics process of inhibitors into PR which are mainly related with the semiopen and open states. Therefore, even the CG treat-ment cannot exclusively define the closed state, it captured the main dynamics factors of the gating of PR and binding process of inhibitors.

For the inhibitor SQV, a largely different topology leads to a quite different binding modes and process from XK263. As shown in Fig. 6, the flaps may open several times before SQV entered the cavity, e.g., in Fig. 7 ($t=21.48$ ns) a flap-opening event (a central wide opening) with failed entering process was shown. Because of the unique topology of SQV, the inhibitor has to seek a proper entrance to the cavity. As shown in Fig. 7 ($t=71.96$ ns), SQV only enters the cavity when the flaps opened large enough (i.e., including the central and lateral motions). Even after SQV enters the cavity, the flaps might reopen quickly (Fig. 7, $t=125.86$ ns) and closed until SQV aligned at the right position (whereas the ILE50A-ILE50B distance remains at about 5 Å, as showed in Fig. 7, $t=181.50$ ns and after). Once the flaps closed, the fluctuations of the flaps and the inhibitor are significantly reduced, and the energy is stabilized at much lower state [Fig. 6(b)] and PR fully bound with the inhibitor.

Interestingly, we observed that the small inhibitors such as XK263 may enter the cavity even with the flaps closed. However large inhibitors such as SQV have to enter with the flaps opened. Apparently SQV-PR needed more time to fully close than XK263-PR. This observation was consistent with the all-atom simulations results.[33,34] We found that for the larger inhibitors like SQV, the binding processes can be classified in a two-step mechanism:[24] First the "diffusion control" step, the inhibitor diffuses to the PR and forms a loosely bound inhibitor-PR complex with the flaps open; second the "gating control" step, accompanying with the closing flaps, a tightly bound complex formed as the flaps closed on the inhibitors. On the other side, small inhibitors like XK263 can enter the cavity even without the flaps opening, and the flaps closed tightly and fast once XK263 is at the right position. The fast kinetics of binding processes of XK263 appears as an approximate one-step "diffusion control" mechanism.[25]

Notably the CG method used in this work can capture the essential dynamics of the protein open-close transitions under the interactions of inhibitors, while the previous CG models only focused on the folding of small protein and short peptides.[43–45] In comparison to the Gaussian network model of HIV-1 PR,[38] this CG dynamics not only reveal the cooperative fluctuations but also the ligand binding dynamics and pathways.

C. Interaction energies and association rate for HIV-1 PR inhibitors

The interaction energies for different HIV-1 PR inhibitors are listed in Table I. The primary driving forces are the contributions of nonbonded interaction between PR and inhibitor, ΔG_{MM}. The nonpolar solvation energy which corresponds to the burial of SASA upon binding contributes much smaller than ΔG_{MM}, and the polar contribution (the polar solvation free energy) served as the primary resistance in the binding processes. Of course, the conformational entropy changes of inhibitors and PR may also have style contributions to binding energy. However they were not accounted in
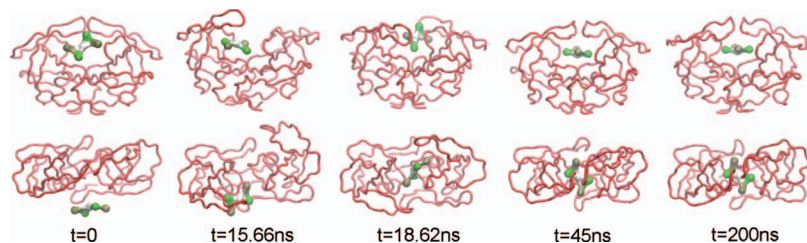
FIG. 5. (Color) Snapshots of the CG simulation of XK263 binding into the active site of HIV-1 PR.

Table I. Therefore the values calculated here are systematically larger than those of experiments. Given the previous studies[30] that the entropic contribution of PR from the open to the closed state was about 11 ± 10 kcal/mol, the binding energies we obtained are in the correct range if taking this into account.

The association rate constants from experiments and the binding time determined from our simulations are showed in Table II. The association rate constants of XK263 was the largest one in the four inhibitors, reached to 10^9–10^{10} M^{-1} s^{-1}. For inhibitor nelfinavir (NFV) and SQV, the association rate constants were at the 10^5–10^6 M^{-1} s^{-1} level. To estimate a binding time using the CG models, the inhibitor XK263 has the fastest kinetics entering with a binding time of about ~15 ns. In contrast, the binding times of other inhibitors were well beyond the level of ~100 ns. The CG models revealed different kinetic rates of varying inhibitors, which were consistent with the experiment data qualitatively.

Experiments indicated that association rate of HIV-1 PR binding substrates or inhibitors are in a wide range of 10^2–10^8 M^{-1} s^{-1}, which are below the diffusion-limited level of 10^9–10^{10} M^{-1} s^{-1}.[20,22,23] Interestingly, the association rates of cyclic urea inhibitors, e.g., inhibitors XK263 and DMP323 are in the range of 10^9–10^{10} M^{-1} s^{-1}, which is close to the diffusion-limited rate.[22] In contrast, the association rate of SQV was about 10^6 M^{-1} s^{-1}, which means the large inhibitor SQV needs the full opening of flaps[22] and binding process is beyond simple diffusion-limited mode. The wide range of the association rate constants reflect that the binding processes are not only diffusion controlled but also influenced by many other factors, such as PR-inhibitor interactions, geometrical constraints of the active site and/or topology of inhibitors.[79] However the details of these influences are not yet understood.

D. The effect of interaction strength on inhibition

For different schemes of binding dynamics and pathways, the main driving force is the nonbond interaction between the inhibitors and the PR cavity. There is indicative trend that the old generation inhibitors (indinavir, NFV, SQV) are entropically driven while the new generation potent inhibitors (amprenavir, lopinavir) are based on more enthalpic binding interactions.[80] For the later case, the flexibility of inhibitor can adapt the subtle conformational changes induced by targeted mutations of PR. However, the more flexible of dynamics, the more would inhibitors lose their conformational entropy upon binding.[81–83] Thus understanding the effect of inhibitors' interaction strength and stiffness is critical to novel inhibitor designs for HIV-1 PR.

To investigate the effect of the interaction strength on the binding dynamics, we mimicked the strength change of the LJ potential between the inhibitor and PR by $\varepsilon = \varepsilon^* \varepsilon_0$ in the potential Eq. (3). Here ε^* is a dimensionless parameter, and ε_0 is the strength of the LJ energy which is from our all-atom calculations of interaction energy. We found that, as shown in Fig. 8, the binding time of inhibitors decreases significantly versus a stronger strength of LJ potential (e.g., when $\varepsilon^* > 1$, the binding time of XK263 would be less than 5 ns; However for SQV, the same scale change of binding time would request $\varepsilon^* > 1.5$).

This gives a dynamics picture on the mode of inhibitors tightly binding with the PR cavity: When the inhibitor diffuses near the cavity, the driving forces of the cavity make the inhibitors collide with the flaps. Once the attraction is
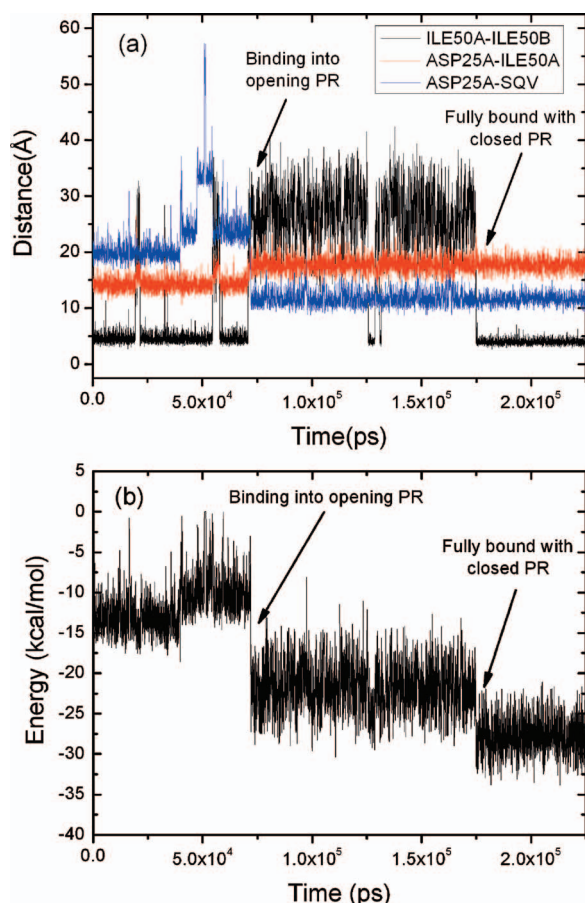

FIG. 6. (Color) Binding dynamics of FDA-approved HIV-1 PR inhibitor SQV. (a) Distances of ILE50A-ILE50B, ASP25A-ILE50A and ASP25A-SQV obtained in the LD simulations with collision frequency 2/ps. (b) The total interaction energy changes during the binding process.
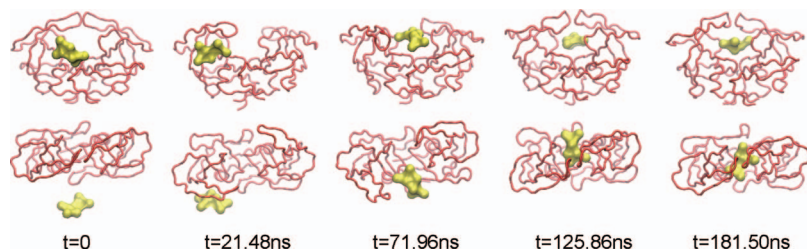
FIG. 7. (Color) Snapshots of the CG simulation of SQV binding into the active site of HIV-1 PR.

strong enough that the inhibitor pushes the flaps opening up (i.e., by an increasing distance of ASP25A-ILE50A), the cavity is open for the inhibitor entering (one extreme case would be an inhibitor entering without flaps opening). As demonstrated by Sadiq *et al.*,[84] the larger inhibitors (e.g., SQV) can be driven out of the cavity by a lateral force where the PR did not show significantly opened configuration. Our work now makes it clearer that lateral inhibitor expulsion from a semiopen configuration is possible. For a comparative process, the inhibitor can enter the PR cavity without the full flaps opening, only if the interaction strength is strong enough. However, if the attraction was weaker, the inhibitors could not open the flaps up, e.g., $\varepsilon^* < 0.5$, the inhibitors may drift away from the PR and this lead to failed binding processes.

It is worthy to note that as the driving forces get weaker, the binding time calculated was more scattered since the stochastic effect would play more dominant roles in the binding dynamics. As shown in the experiment data, the binding kinetics of small inhibitors (e.g., XK263 of Table I) is much faster than larger inhibitors. It is due to that the strong interaction strength would overcome the conformational entropy restrictions. On the other side, when the attraction between inhibitor and PR becomes strong, the inhibitor dynamics would heavily affect the PR dynamics, i.e., enlarging the entrance or opening of the flaps. This reminds us, the inhibitor flexibility will dynamically affect the inhibition binding process: For very flexible or small inhibitors, it can change its shape to adapt the narrow entrance to PR by simple attractions (one-step binding, i.e., diffusion limited). In contrast, if the inhibitor was stiff or large, the strong attractions would push the PR flaps for a wide entrance and the inhibitors must wait for the flaps' full opening to enter, and this leads to the two-step binding (i.e., diffusion-limited and gating controlled).

Similar to the binding behaviors of the HIV-1 PR system, the above analyses can also be applied to other protein translocation processes, e.g., through the nanopore.[85,86] In nanopores, the molecules such as small protein segments may be induced to unfold before entering the pore.[85] Similarly, a single-stranded DNA helix can be unstacked by the nanopore.[86] In both situations, like HIV-1 PR, the competition of the driving forces and the deformability of entering molecules control the translocation processes.

IV. CONCLUSIONS

We implemented a CG dynamics algorithm to simulate protein-ligand dynamics at very large timescales up to microsecond. We calculated the interaction energy with the all-

atom simulation and obtain the interaction parameters in CG dynamics. This CG dynamics was successfully tested in the inhibition dynamics of HIV-1 PR and its ligands. CG dynamics shows same level of accuracy as all-atom simulation in term of fluctuations, collective motions, and binding pathways.

A notable finding in HIV-1 PR is that ILE50A-ILE50B and ASP25A-ILE50A distances correlated positively in the bound-free PR or the inhibitor-binding PR. The binding times calculated in the CG simulation were consistent with the association rate constants from experiments. We also find the binding processes of different inhibitors can be classified
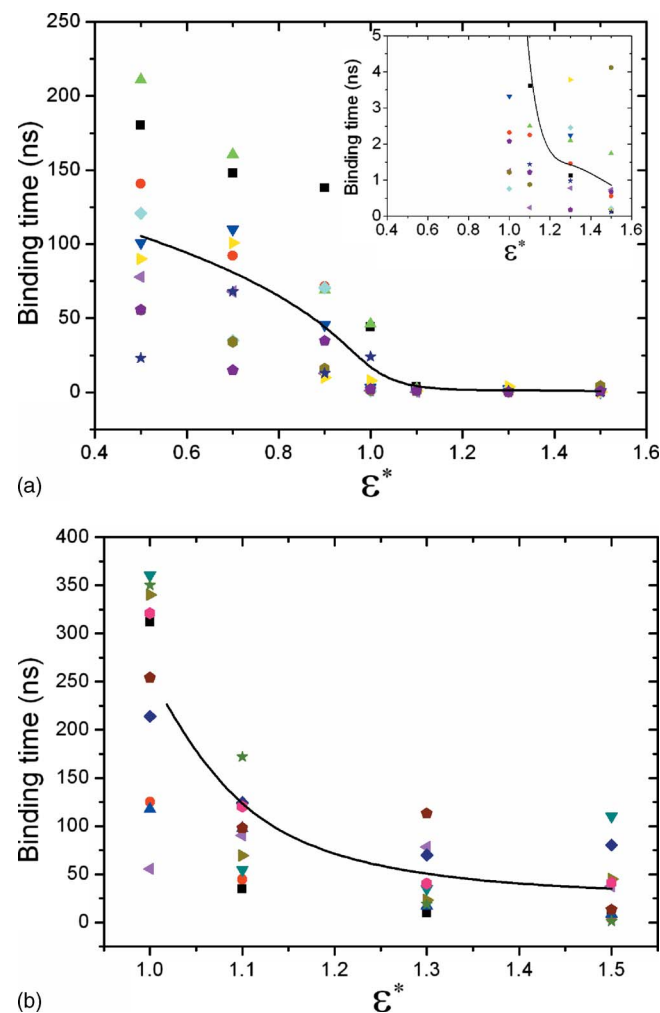

FIG. 8. (Color online) Inhibition binding time depends on the varied interaction strength for CG model of (a) XK263 (with an inset with more details) and (b) SQV. The binding time was defined from the beginning of simulation to the inhibitor entered the cavity with the flaps closed. The data points were distinct simulations with different initial velocity but the same initial position of inhibitors. The solid line was the average times.

into two types: The one-step scheme controlled by diffusion only and the two-step scheme controlled by both diffusion and the gating of PR flaps. For different schemes of binding dynamics and pathways, the driving force is the nonbond interaction between the inhibitors and the PR cavity. Meanwhile, the size and topology of inhibitors and the interaction strength between inhibitors and PR have great influence on the binding dynamics. Compared to previous studies, this work provides a more quantitative dynamics study on binding behaviors of inhibitors into PR.

ACKNOWLEDGMENTS

[1] K. A. Henzler-Wildman, T. Vu, L. Ming, M. Ott, M. Wolf-Watz, T. Fenn, E. Pozharski, M. A. Wilson, G. A. Petsko, M. Karplus, C. G. Hubner, and D. Kerr, Nature (London) **450**, 838 (2007).
[2] D. Kern and E. R. P. Zuiderweg, Curr. Opin. Struct. Biol. **13**, 748 (2003).
[3] C.-J. Tsai, A. del Sol, and R. Nussinov, J. Mol. Biol. **378**, 1 (2008).
[4] J. A. Hardy and J. A. Wells, Curr. Opin. Struct. Biol. **14**, 706 (2004).
[5] R. A. Katz and A. M. Skalka, Annu. Rev. Biochem. **63**, 133 (1994).
[6] P. P. Mager, Med. Res. Rev. **21**, 348 (2001).
[7] D. C. Chatfield and B. R. Brooks, J. Am. Chem. Soc. **117**, 5561 (1995).
[8] N. E. Kohl, E. A. Emini, W. A. Schleif, L. J. Davis, J. C. Heimbach, R. A. F. Dixon, E. M. Scolnick, and I. S. Sigal, Proc. Natl. Acad. Sci. U.S.A. **85**, 4686 (1988).
[9] A. Wlodawer and J. Vondrasek, Annu. Rev. Biophys. Biomol. Struct. **27**, 249 (1998).
[10] V. Hornak and C. Simmerling, Drug Discovery Today **12**, 132 (2007).
[11] T. Ridky and J. Leis, J. Biol. Chem. **270**, 29621 (1995).
[12] J. H. Condra, W. A. Schleif, O. M. Blahy, L. J. Gabryelski, D. J. Graham, J. C. Quintero, A. Rhodes, H. L. Robbins, E. Roth, M. Shivaprakash, D. Titus, T. Yang, H. Teppler, K. E. Squires, P. J. Deutsch, and E. A. Emini, Nature (London) **374**, 569 (1995).
[13] S. Spinelli, Q. Z. Liu, P. M. Alzari, P. H. Hirel, and R. J. Poljak, Biochimie **73**, 1391 (1991).
[14] P. Y. S. Lam, P. K. Jadhav, C. J. Eyermann, C. N. Hodge, Y. Ru, L. T. Bacheler, J. L. Meek, M. J. Otto, M. M. Rayner, Y. N. Wong, C. H. Chang, P. C. Weber, D. A. Jackson, T. R. Sharpe, and S. Ericksonviitanen, Science **263**, 380 (1994).
[15] M. Prabu-Jeyabalan, E. Nalivaika, and C. A. Schiffer, J. Mol. Biol. **301**, 1207 (2000).
[16] P. Martin, J. F. Vickrey, G. Proteasa, Y. L. Jimenez, Z. Wawrzak, M. A. Winters, T. C. Merigan, and L. C. Kovari, Structure (London) **13**, 1887 (2005).
[17] M. Layten, V. Hornak, and C. Simmerling, J. Am. Chem. Soc. **128**, 13360 (2006).
[18] R. Ishima, D. I. Freedberg, Y. X. Wang, J. M. Louis, and D. A. Torchia, Structure (London) **7**, 1047 (1999).
[19] D. I. Freedberg, R. Ishima, J. Jacob, Y. X. Wang, I. Kustanovich, J. M. Louis, and D. A. Torchia, Protein Sci. **11**, 221 (2002).
[20] E. Katoh, J. M. Louis, T. Yamazaki, A. M. Gronenborn, D. A. Torchia, and R. Ishima, Protein Sci. **12**, 1376 (2003).
[21] L. K. Nicholson, T. Yamazaki, D. A. Torchia, S. Grzesiek, A. Bax, S. J. Stahl, J. D. Kaufman, P. T. Wingfield, P. Y. S. Lam, P. K. Jadhav, C. N. Hodge, P. J. Domaille, and C. H. Chang, Nat. Struct. Biol. **2**, 274 (1995).
[22] P. O. Markgren, W. Schaal, M. Hamalainen, A. Karlen, A. Hallberg, B. Samuelsson, and U. H. Danielson, J. Med. Chem. **45**, 5430 (2002).
[23] Y. H. Song, Y. J. Zhang, T. Y. Shen, C. L. Bajaj, A. McCammon, and N. A. Baker, Biophys. J. **86**, 2017 (2004).
[24] E. S. Furfine, E. Dsouza, K. J. Ingold, J. J. Leban, T. Spector, and D. J. T. Porter, Biochemistry **31**, 7886 (1992).
[25] E. J. Rodriguez, C. Debouck, I. C. Deckman, H. Abusoud, F. M. Raushel, and T. D. Meek, Biochemistry **32**, 3557 (1993).
[26] S. Piana, P. Carloni, and M. Parrinello, J. Mol. Biol. **319**, 567 (2002).
[27] J. R. Collins, S. K. Burt, and J. W. Erickson, Nat. Struct. Biol. **2**, 334 (1995).
[28] W. R. P. Scott and C. A. Schiffer, Structure (London) **8**, 1259 (2000).
[29] G. Toth and A. Borics, J. Mol. Graphics Modell. **24**, 465 (2006).
[30] S. W. Rick, J. W. Erickson, and S. K. Burt, Proteins: Struct., Funct., Bioinf. **32**, 7 (1998).
[31] V. Hornak, A. Okur, R. C. Rizzo, and C. Simmerling, Proc. Natl. Acad. Sci. U.S.A. **103**, 915 (2006).
[32] J. Trylska, V. Tozzini, C. A. Chang, and J. A. McCammon, Biophys. J. **92**, 4179 (2007).
[33] G. Toth and A. Borics, Biochemistry **45**, 6606 (2006).
[34] V. Hornak, A. Okur, R. C. Rizzo, and C. Simmerling, J. Am. Chem. Soc. **128**, 2812 (2006).
[35] V. Tozzini, Curr. Opin. Struct. Biol. **15**, 144 (2005).
[36] S. Brown, N. J. Fawzi, and T. Head-Gordon, Proc. Natl. Acad. Sci. U.S.A. **100**, 10712 (2003).
[37] T. Haliloglu, I. Bahar, and B. Erman, Phys. Rev. Lett. **79**, 3090 (1997).
[38] N. Kurt, W. R. P. Scott, C. A. Schiffer, and T. Haliloglu, Proteins: Struct., Funct., Genet. **51**, 409 (2003).
[39] N. Kurt, T. Haliloglu, and C. A. Schiffer, Biophys. J. **85**, 853 (2003).
[40] A. R. Lam, J. M. Borreguero, F. Ding, N. V. Dokholyan, S. V. Buldyrev, H. E. Stanley, and E. Shakhnovich, J. Mol. Biol. **373**, 1348 (2007).
[41] S. Takada, Z. Luthey-Schulten, and P. G. Wolynes, J. Chem. Phys. **110**, 11616 (1999).
[42] A. Wallqvist and M. Ullner, Proteins: Struct., Funct., Genet. **18**, 267 (1994).
[43] A. Voegler Smith and C. K. Hall, Proteins: Struct., Funct., Genet. **44**, 344 (2001).
[44] F. Ding, J. M. Borreguero, S. V. Buldyrev, H. E. Stanley, and N. V. Dokholyan, Proteins: Struct., Funct., Genet. **53**, 220 (2003).
[45] B. Urbanc, L. Cruz, F. Ding, D. Sammond, S. Khare, S. V. Buldyrev, H. E. Stanley, and N. V. Dokholyan, Biophys. J. **87**, 2310 (2004).
[46] A. Irback, F. Sjunnesson, and S. Wallin, Proc. Natl. Acad. Sci. U.S.A. **97**, 13614 (2000).
[47] V. Tozzini and J. A. McCammon, Chem. Phys. Lett. **413**, 123 (2005).
[48] V. Tozzini, J. Trylska, C. E. Chang, and J. A. McCammon, J. Struct. Biol. **157**, 606 (2007).
[49] C. E. Chang, T. Shen, J. Trylska, V. Tozzini, and J. A. McCammon, Biophys. J. **90**, 3880 (2006).
[50] D. D. L. Minh, C. E. Chang, J. Trylska, V. Tozzini, and J. A. McCammon, J. Am. Chem. Soc. **128**, 6006 (2006).
[51] C. E. A. Chang, J. Trylska, V. Tozzini, and J. A. McCammon, Chem. Biol. Drug Des. **69**, 5 (2007).
[52] B. A. Reva, A. V. Finkelstein, M. F. Sanner, and A. J. Olson, Protein Eng. **10**, 865 (1997).
[53] M. Zacharias, Protein Sci. **12**, 1271 (2003).
[54] A. K. Rappe, C. J. Casewit, K. S. Colwell, W. A. Goddard, and W. M. Skiff, J. Am. Chem. Soc. **114**, 10024 (1992).
[55] P. A. Kollman, I. Massova, C. Reyes, B. Kuhn, S. H. Huo, L. Chong, M. Lee, T. Lee, Y. Duan, W. Wang, O. Donini, P. Cieplak, J. Srinivasan, D. A. Case, and T. E. Cheatham, Acc. Chem. Res. **33**, 889 (2000).
[56] N. A. Baker, D. Sept, S. Joseph, M. J. Holst, and J. A. McCammon, Proc. Natl. Acad. Sci. U.S.A. **98**, 10037 (2001).
[57] T. J. Dolinsky, J. E. Nielsen, J. A. McCammon, and N. A. Baker, Nucleic Acids Res. **32**, W665 (2004).
[58] M. F. Sanner, A. J. Olson, and J. C. Spehner, Biopolymers **38**, 305 (1996).
[59] D. Sitkoff, K. A. Sharp, and B. Honig, J. Phys. Chem. **98**, 1978 (1994).
[60] W. Wang and P. A. Kollman, Proc. Natl. Acad. Sci. U.S.A. **98**, 14937 (2001).
[61] E. Lindahl, B. Hess, and D. van der Spoel, J. Mol. Model. **7**, 306 (2001).
[62] H. J. C. Berendsen, D. Vanderspoel, and R. Vandrunen, Comput. Phys. Commun. **91**, 43 (1995).
[63] W. Smith, C. W. Yong, and P. M. Rodger, Mol. Simul. **28**, 385 (2002).
[64] M. E. Davis, J. D. Madura, B. A. Luty, and J. A. McCammon, Comput. Phys. Commun. **62**, 187 (1991).
[65] S. W. Kaldor, V. J. Kalish, J. F. Davies, B. V. Shetty, J. E. Fritz, K.

Appelt, J. A. Burgess, K. M. Campanale, N. Y. Chirgadze, D. K. Clawson, B. A. Dressman, S. D. Hatch, D. A. Khalil, M. B. Kosa, P. P. Lubbehusen, M. A. Muesing, A. K. Patick, S. H. Reich, K. S. Su, and J. H. Tatlock, J. Med. Chem. **40**, 3979 (1997).

[66] A. Krohn, S. Redshaw, J. C. Ritchie, B. J. Graves, and M. H. Hatada, J. Med. Chem. **34**, 3340 (1991).

[67] J. Weber, J. R. Mesters, M. Lepsik, J. Prejdova, M. Svec, J. Sponarova, P. Mlcochova, K. Skalicka, K. Strisovsky, T. Uhlikova, M. Soucek, L. Machala, M. Stankova, J. Vondrasek, T. Klimkait, H. G. Kraeusslich, R. Hilgenfeld, and J. Konvalinka, J. Mol. Biol. **324**, 739 (2002).

[68] E. J. Sorin and V. S. Pande, Biophys. J. **88**, 2472 (2005).

[69] J. Wang, W. Wang, P. A. Kollman, and D. A. Case, J. Mol. Graphics Modell. **25**, 247 (2006).

[70] J. M. Wang, R. M. Wolf, J. W. Caldwell, P. A. Kollman, and D. A. Case, J. Comput. Chem. **25**, 1157 (2004).

[71] A. Jakalian, B. L. Bush, D. B. Jack, and C. I. Bayly, J. Comput. Chem. **21**, 132 (2000).

[72] D. A. Case, T. E. Cheatham, T. Darden, H. Gohlke, R. Luo, K. M. Merz, A. Onufriev, C. Simmerling, B. Wang, and R. J. Woods, J. Comput. Chem. **26**, 1668 (2005).

[73] W. L. Jorgensen, J. Chandrasekhar, J. D. Madura, R. W. Impey, and M. L. Klein, J. Chem. Phys. **79**, 926 (1983).

[74] U. Essmann, L. Perera, M. L. Berkowitz, T. Darden, H. Lee, and L. G. Pedersen, J. Chem. Phys. **103**, 8577 (1995).

[75] H. J. C. Berendsen, J. P. M. Postma, W. F. Vangunsteren, A. Dinola, and J. R. Haak, J. Chem. Phys. **81**, 3684 (1984).

[76] J. P. Ryckaert, G. Ciccotti, and H. J. C. Berendsen, J. Comput. Phys. **23**, 327 (1977).

[77] W. Humphrey, A. Dalke, and K. Schulten, J. Mol. Graph. **14**, 33 (1996).

[78] X. Chen, Y. Lin, M. Liu, and M. K. Gilson, Bioinformatics **18**, 130 (2002).

[79] G. Schreiber, Curr. Opin. Struct. Biol. **12**, 41 (2002).

[80] H. Ohtaka, S. Muzammil, A. Schon, A. Velazquez-Campoy, S. Vega, and E. Freire, Int. J. Biochem. Cell Biol. **36**, 1787 (2004).

[81] I. Luque, M. J. Todd, J. Gomez, N. Semo, and E. Freire, Biochemistry **37**, 5791 (1998).

[82] S. Vega, L. W. Kang, A. Velazquez-Campoy, Y. Kiso, L. M. Amzel, and E. Freire, Proteins: Struct., Funct., Bioinf. **55**, 594 (2004).

[83] C. E. A. Chang, W. Chen, and M. K. Gilson, Proc. Natl. Acad. Sci. U.S.A. **104**, 1534 (2007).

[84] A. K. Sadiq, S. Wan, and P. V. Coveney, Biochemistry **46**, 14865 (2007).

[85] R. Stefureac, L. Waldner, P. Howard, and J. S. Lee, Small **4**, 59 (2008).

[86] P. Chen and C. M. Li, Small **3**, 1204 (2007).

[87] See EPAPS Document No. E-JCPSA6-130-019923 for CG force field parameters of various HIV-1 PR inhibitors. For more information on EPAPS, see http://www.aip.org/pubservs/epaps.html.